the FEBS Journal

Identification and functional characterization of an aggregation domain in long myosin light chain kinase

Wen-Cheng Zhang[1], Ya-Jing Peng[1], Wei-Qi He[1], Ning Lv[2], Chen Chen[1], Gang Zhi[3], Hua-Qun Chen[2] and Min-Sheng Zhu[1]

1 Model Animal Research Center, Nanjing University, China
2 School of Life Science, Nanjing Normal University, China
3 National Institute of Biological Science, Beijing, China

Keywords
4Ig domain; aggregation; contraction; mitochondria; myosin light chain kinase

Correspondence
M.-S. Zhu, Model Animal Research Center of Nanjing University, 12 Xue-Fu Road, Pukou District, Nanjing, China 210061
Fax: +86 2558641500
Tel: +86 2558641529
E-mail: zhums@nju.edu.cn

(Received 14 January 2008, revised 4 March 2008, accepted 11 March 2008)

doi:10.1111/j.1742-4658.2008.06393.x

The functions of long smooth muscle myosin light chain kinase (L-MLCK), a molecule with multiple domains, are poorly understood. To examine the existence of further potentially functional domains in this molecule, we analyzed its amino acid sequence with a TANGO program and found a putative aggregation domain located at the 4Ig domain of the N-terminal extension. To verify its aggregation capability *in vitro*, expressible truncated L-MLCK variants driven by a cytomegalovirus promoter were transfected into cells. As anticipated, only the overexpression of the 4Ig fragment led to particle formation in Colon26 cells. These particles contained 4Ig polymers and actin. Analysis with detergents demonstrated that the particles shared features in common with aggregates. Thus, we conclude that the 4Ig domain has a potent aggregation ability. To further examine this aggregation domain *in vivo*, eight transgenic mouse lines expressing the 4Ig domain (4Ig lines) were generated. The results showed that the transgenic mice had typical aggregation in the thigh and diaphragm muscles. Histological examination showed that 7.70 ± 1.86% of extensor digitorum longus myofibrils displayed aggregates with a 36.44% reduction in myofibril diameter, whereas 65.13 ± 3.42% of diaphragm myofibrils displayed aggregates and the myofibril diameter was reduced by 43.08%. Electron microscopy examination suggested that the aggregates were deposited at the mitochondria, resulting in structural impairment. As a consequence, the oxygen consumption of mitochondria in the affected muscles was also reduced. Macrophenotypic analysis showed the presence of muscular degeneration characterized by a reduction in force development, faster fatigue, decreased myofibril diameters, and structural alterations. In summary, our study revealed the existence of a novel aggregation domain in L-MLCK and provided a direct link between L-MLCK and aggregation. The possible significance and mechanism underlying the aggregation-based pathological processes mediated by L-MLCK are also discussed.

Myosin light chain kinases (MLCKs) activate myosin by phosphorylating Thr18 and Ser19 on the regulatory light chain of myosin II [1–3]. The phosphorylated myosin II has increasingly been shown to be involved in many physiological processes, including cell spreading and migration, the extension of neurite growth

Abbreviations
CMV, cytomegalovirus; CMVIE, cytomegalovirus immediate element 1; EDL, extensor digitorum longus; EGFP, enhanced green fluorescent protein; GFP, green fluorescent protein; HSP, heat shock protein; L-MLCK, long smooth muscle myosin light chain kinase; MLCK, myosin light chain kinase; RCR, respiratory control ratio; skMLCK, skeletal muscle myosin light chain kinase; S-MLCK, short myosin light chain kinase; smMLCK, smooth muscle myosin light chain kinase; TEF, toxicity equivalency factor.

cones, cytokinesis and cytoskeletal clustering of integrins at focal adhesions, stress fiber formation, changes in platelet shape, secretion, exocytosis and transepithelial permeability [4–15]. In vertebrates, there are two MLCK genes at different genomic loci; those encoding skeletal muscle MLCK (skMLCK) and smooth muscle MLCK (smMLCK) [3]. smMLCK is the product of a single gene, distinct from the gene giving rise to skMLCK [4]. Long smMLCK (L-MLCK; 208–214 kDa in length) and short smMLCK (S-MLCK; 130–150 kDa in length) are two isoforms resulting from different transcripts initiated at different promoters at the same locus [16].

L-MLCK is identical to S-MLCK except for the presence of a unique N-terminal extension that contains several extra structural motifs, including a 2Ig domain at the distal N-terminus and a 4Ig domain and DFRxxL motif at the proximal N-terminus [16,17]. These structural differences may account for the differential functioning of the MLCK isoforms. However, the functions of L-MLCK are poorly understood. Investigating the existence of potentially functional domains in this extension is of importance for elucidating the roles of L-MLCK. Some functional domains have already been identified in L-MLCK and, on the basis of their biochemical properties and functional characteristics, potential roles have been proposed. These include a role in cytoskeletal reorganization through DFRxxL and/or the 2Ig domain, and a regulatory role during mitosis through the N-terminal extension [18–20]. Whether L-MLCK has further functional domains and whether the 4Ig motif itself has a potential function remain unknown. In this work, a putative aggregation domain within the 4Ig motif was identified using a TANGO program. The potent aggregation ability of this domain was demonstrated by both *in vitro* and *in vivo* analysis. The aggregation properties and possible functions were also characterized. Our results suggest a novel aggregation domain within the N-terminal extension of L-MLCK. In addition, a preliminary mechanism underlying the aggregation-based pathological processes mediated by L-MLCK and the possible involvement of heat shock protein (HSP) in aggregate formation are proposed.

Results

L-MLCK contained a putative aggregation region in the N-terminal extension

Full-length sequences of L-MLCK were subjected to TANGO program interrogation in INTRINSIC PROTEIN DISORDER PREDICTION 1.4 with default parameters [21]. A conserved aggregation motif was revealed within 4Ig, the sequence of which varied across species (e.g. VFTLVL, VCIWAVFYW and LVLLIVL) (Fig. 1A). There was a weak aggregation motif within the 1Ig region of chicken MLCK. An aggregation motif outside of the 4Ig region was found in both rat and primate L-MLCKs, but this was not conserved across the species. Our preliminary data showed no aggregation ability of this motif in cultured cells (data not shown), and we therefore focused on examining the aggregation domain within the 4Ig region in our subsequent experiments.

Overexpression of the 4Ig fragment elicited protein aggregation *in vitro*

To determine the aggregation ability of the 4Ig fragment, an expressible vector (pC3–4Ig) was produced by fusing the 4Ig-coding region in the C-terminus of the enhanced green fluorescent protein (EGFP) gene driven by the cytomegalovirus (CMV) promoter (Fig. 1B). After transfection of the vector into Colon26 cells, visible fluorescent particles, which were identified as protein aggregates in our subsequent experiments, were observed in the cells (Fig. 2A,B). The fluorescent particles accumulated in a time-dependent manner. Nine hours after transfection, about 16.7% of transfected cells contained such particles, and by 12 h, the ratio had increased to 35.4%. When 4Ig was fused with the N-terminus of EGFP (pEGFP–4Ig) (Fig. 1B), a similar result was observed (data not shown). Neither full-length L-MLCK (pEGFP–MLCK210) nor chicken 2Ig (pEGFP215) caused any aggregation under the same experimental conditions (Fig. 2A).

After sequential treatments with Triton X-100 and SDS, most particles remained visible for at least 30 min and then slowly dissolved, showing the typical detergent-resistant property of aggregates. In control cells expressing the EGFP protein, Triton X-100 eliminated fluorescence completely from the cell body (Fig. 2B). This detergent-resistant property of the aggregates was confirmed by western blot assay, and similar conclusions were reached (Fig. 2C). Thus, this result suggests that the particle is a protein aggregate.

4Ig elicited protein aggregation *in vivo*

To verify the aggregation domain *in vivo*, eight founders, and subsequently eight stable lines (4Ig-Tg: 1–8) with pC3–4Ig integration, were obtained by genotypic screening with PCR with primers specific to EGFP. Protein expression was determined by western blot assay. All but line 4Ig-Tg-2 expressed 4Ig in the

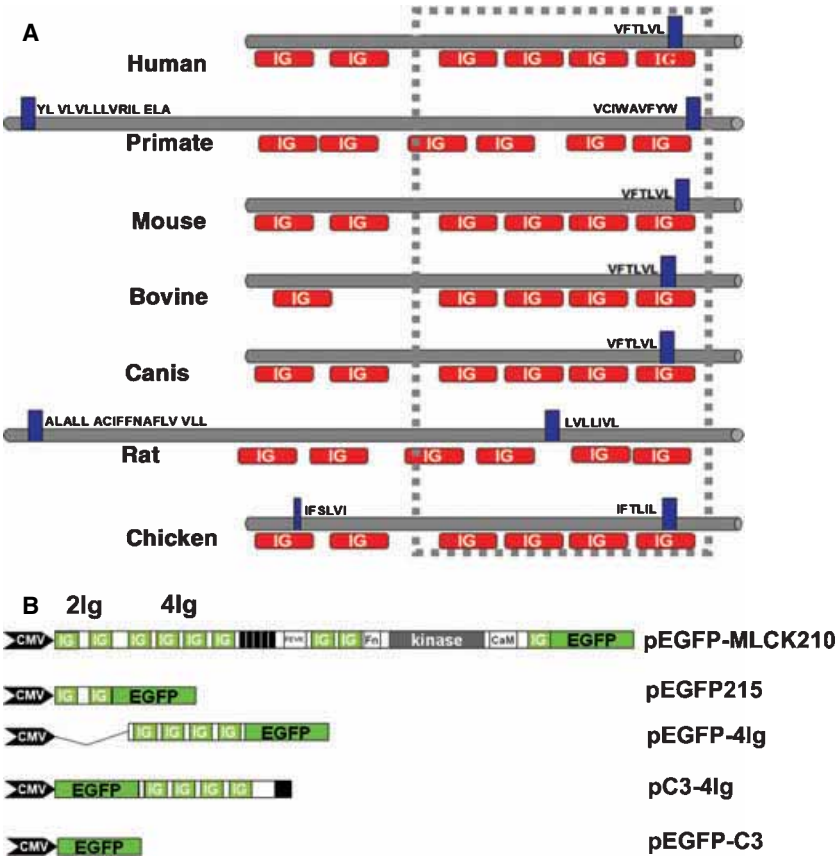

Fig. 1. Prediction for a conserved aggregation domain in the 4Ig region of L-MLCK and recombinant expression of MLCK variants. (A) The sequences of the N-terminal extension of L-MLCK were subjected to domain prediction in the NCBI ENTREZ program for identifying Ig-like modules, and then entered into the TANGO program (http://dis.embl.de/) for predicting beta aggregation sequences (the parameters were: pH 7.4; temperature 278.15 K; ion strength 0.05 M; toxicity equivalency factor (TEF) concentration 0 M; and TANGO threshold 1). Solid rectangles represent aggregation-prone regions, and red rectangles represent putative Ig-like modules. (B) MLCK constructs. The construction details for pEGFP–MLCK210, pEGFP215 and pEGFP–4Ig are given in our previous report [19]. To make the pC3–4Ig plasmid, the 4Ig region was amplified by PCR and subcloned into the pEGFP–C3 expression vector.

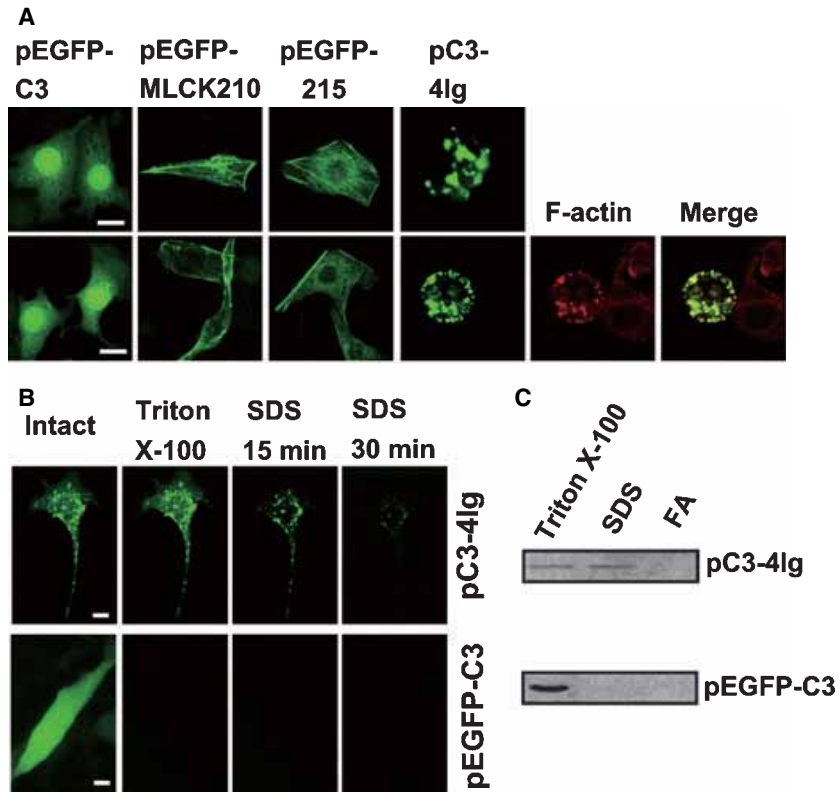

Fig. 2. Aggregate formation in the cells expressing MLCK variants. (A) Different MLCK variants were transfected into Colon26 cells with Lipofectamine 2000 (Invitrogen). The transfected cells were examined under a laser confocal scanning microscope (LCSM; Leica-SP2, Leica, Germany). Actin in cells showing aggregation was then stained with rhodamine-labeled phalloidin. The internal marker measures 20 μm. (B) Colon26 cells were transfected with pC3–4Ig or pEGFP–C3. Twenty-four hours after transfection, the cells were treated with 1% Triton X-100 for 30 min and then with 2% SDS. The internal marker measures 20 μm above and 8 μm below. (C) About 1×10^6 cells transfected with pC3–4Ig or pEGFP–C3 were harvested and treated sequentially with 1% Triton X-100, 2% SDS and 70% formic acid (FA), together with 2% SDS. Centrifugation was performed after each treatment step. The supernatants were subjected to western blot assay to measure the amount of recombinant proteins. These experiments were repeated independently at least four times.

skeletal muscle. In line 4Ig-Tg-2, 4Ig was expressed only in the heart and lungs. Line 4Ig-Tg-7 expressed 4Ig in the skeletal muscle and spleen. Little expression of 4Ig was detected in the intestinal epithelium, liver and heart of mice from lines 4Ig-Tg-1, 4Ig-Tg-3, 4Ig-Tg-4, and 4Ig-Tg-6. After backcrossing to C57BL/6 for four generations, transgenic mice exhibited similar expression patterns of recombinant 4Ig. Figure 3A shows a typical expression pattern in different lines, in which the level of expression of 4Ig varied both within the same tissues of different lines and between different tissues in the same line.

To examine tissue aggregates, various fresh tissues were fixed with 4% paraformaldehyde in NaCl/P_i for 30 min, and tissue slides of $\sim$ 200 μm thickness were observed under a confocal microscope. Putative aggregates were found in skeletal myofibrils, including in the muscles of the thigh and diaphragm (Fig. 3B,C). Low expression of 4Ig in skeletal muscle (such as in line 1) also caused the formation of a clear aggregate. The ratio of aggregate-containing fibers to normal fibers was about 7.7% in the extensor digitorum longus (EDL) muscle. No visible aggregates occurred in the other tissues, including the heart, liver and kidney (not shown). In the EGFP transgenic control [C57BL/6-Tg(CAG-EGFP)C14-Yol-FM131Osb, referred to as EGFP-Tg in this article], no visible aggregate was detected in the skeletal muscle, heart, liver, intestine, brain or kidney.

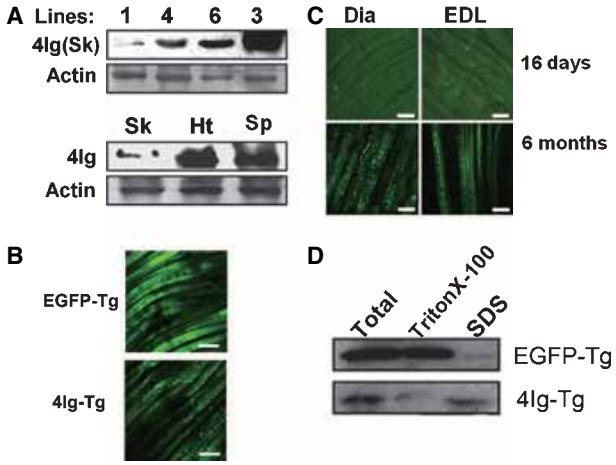

Fig. 3. Expression and aggregate formation of 4Ig in transgenic mice. (A) Skeletal muscle from different lines (upper panel) and skeletal muscle, heart and spleen tissues (lower panel) were sampled for western blot assay with antibody to GFP. Total actin was stained with Coomassie blue as a loading control. Sk, skeletal muscle; Ht, heart; Sp, spleen. (B) Fresh EDL muscle was carefully torn into pieces along the length of the myofibers, fixed with 4% paraformaldehyde for 30 min, and washed three times with NaCl/P_i. The samples were then examined under a confocal microscope. 4Ig-Tg, transgenic mice expressing 4Ig; GFP-Tg, transgenic mice expressing EGFP. (C) Aggregation in muscles of different ages. Diaphragm and EDL muscles were dissected from 4Ig-transgenic mice at different ages (16 days old and 6 months old) and examined under a confocal microscope. Dia, diaphragm muscle. The internal marker measures 100 μm. (D) Approximately 10 mg of muscle tissue was homogenized and treated sequentially with 1% Triton X-100 and 2% SDS. The recombinant proteins were measured by western blot assay. The soluble proteins were subjected to western blot assay with antibody to GFP.

In order to determine the biochemical features of the aggregates, muscle homogenates were sequentially treated with Triton X-100 and SDS. The supernatant-dissolved 4Ig protein was measured by western blot assay. The results showed that 4Ig aggregates in skeletal muscle fibers were resistant to Triton X-100 and partially soluble in SDS (Fig. 3D), showing one of the typical features of aggregates. Interestingly, in diaphragm muscle, more intensive aggregation was observed (Fig. 3C), suggesting that this tissue more readily allows 4Ig aggregation.

To characterize the 4Ig aggregations *in vitro*, we purified refolded recombinant 4Ig protein (monomer) and then treated it with H_2O_2, which acted as an oxidative stress, according to previously described methods [22,23]. The results showed evidence of clear multimer formation after addition of H_2O_2 (Fig. 4A). 4Ig polymer formation could also be confirmed in transgenic diaphragms. The aggregates from different lines contained 4Ig polymers, but no polymer was detected in the transgenic spleen control (Fig. 4B). Thus, the formation of 4Ig protein polymers may be an important process in the development of 4Ig aggregates. To investigate whether other ingredients existed in the aggregate, we stained the aggregates in cells with phalloidin, and this revealed the presence of strong actin-staining signals colocalizing with the aggregates (Fig. 2A), suggesting that the actin protein was enriched with 4Ig aggregate.

HSPs have been implicated in aggregate formation. To investigate the potential involvement of HSPs in 4Ig aggregation, we examined HSP73, a constitutive HSP, in aggregate-forming cells or tissues. The results showed that HSP expression was significantly reduced in 4Ig-Tg intestinal tissue, diaphragm and 4Ig-expressing

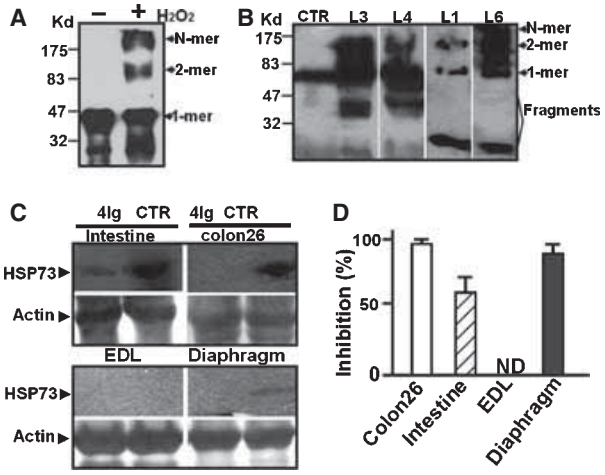

Fig. 4. Characterization of the aggregates. (A) 4Ig polymerization was triggered by H_2O_2 *in vitro*. Native recombinant proteins (4Ig or 2Ig) were purified from soluble lysates of recombinant *Escherichia coli* and treated with or without 50 μM H_2O_2 *in vitro* for 4 h, and then subjected to western blot assay with antibody to 4Ig or antibody to 2Ig. The signals below the monomer indicate degraded protein. (B) 4Ig aggregates from 4Ig-Tg diaphragm (line 3) were analyzed by western blot. Monoclonal antibody to GFP was used as the primary antibody. 4Ig-Tg spleen of line 7 was used as a control (CTR). Arrows indicate monomers, dimers, and multimers. (C) HSP73 expression in 4Ig-expressing tissues and cells. The tissue or cell samples were resolved by 10% SDS/PAGE and assayed by western blot with polyclonal antibody to HSP73 (Sigma-Aldrich, St Louis, MO, USA). Total actin was stained by Coomassie blue for loading the control. (D) The percentages of inhibition of HSP73 by 4Ig expression were quantified. As no HSP73 expression was detected in either 4Ig-expressing or non-4Ig-expressing EDL muscle, the inhibition percentage was not determined (ND).

Colon26 cells (Fig. 4C,D). HSP expression in EDL was still undetectable.

Morphological analysis revealed that the diameters of the affected diaphragm myofibrils decreased from 47.44 μm in the controls to 27.00 μm ($P < 0.01$), whereas the diameters of the affected EDL myofibers decreased from 52.96 μm in the controls to 33.66 μm ($P < 0.01$) (Fig. 6A). The aggregates in the diaphragm exhibited similar biochemical features to those in the EDL samples (data not shown).

4Ig aggregates disrupted mitochondrial structure and functioning

Electron microscopic images showed many aggregate particles occupying mitochondria (Fig. 5A). In these cases, most of the mitochondrial structures had disappeared, and some incomplete mitochondrial membranes remained around the aggregate particles. To determine the extent of mitochondrial functionality, the oxygen consumption of muscles was measured. The oxygen consumption of state 3 respiration in transgenic diaphragm muscles decreased significantly (from 207.6 ± 25.5 nmol $O_2 \cdot min^{-1} \cdot mg^{-1}$ of control muscle to 145.5 ± 21.9 nmol $O_2 \cdot min^{-1} \cdot mg^{-1}$ of transgenic muscle) ($P < 0.05$), whereas it did not change in EDL muscles (227.4 ± 28.3 versus 201.4 ± 10.2 nmol $O_2 \cdot min^{-1} \cdot mg^{-1}$, $P > 0.05$) (Fig. 5B, upper panel). There was no difference between transgenic and control EDL or diaphragm muscles in oxygen consumption during state 4 respiration. Respiratory control ratio (RCR) values in transgenic diaphragm muscles were significantly lower than those in controls (2.1 ± 0.19 versus 2.9 ± 0.17, $P < 0.05$), whereas no difference was observed in RCR values between transgenic and control EDL muscles (2.4 ± 0.077 versus 2.8 ± 0.32, $P > 0.05$) (Fig. 5B, lower panel). Thus, oxygen consumption in transgenic diaphragm muscles was impaired more severely than that in EDL muscle. However, although the impairment in EDL muscle was slight, it was sufficient to affect muscular contractility (see below).

4Ig aggregation caused muscle degeneration

As mentioned above, the aggregate-containing fibers were of small size and irregular morphology, both typical of degenerative pathology. In order to assess the extent of functional degeneration of these muscles, the contraction force of EDL muscle in response to a 10 mA stimulus was measured. The results showed that the force tension decreased from 5.019 ± 0.212 to 4.550 ± 0.068 $N \cdot cm^{-2}$ as compared with littermate controls. Similarly, the isometric twitch force of transgenic diaphragm samples was 2.532 ± 0.232 $N \cdot cm^{-2}$, significantly lower than that of controls (3.288 ± 0.152 $N \cdot cm^{-2}$, $P < 0.05$) (Fig. 6B,C).

A fatigue test was performed to test the fatigue sensitivity of the muscles. Transgenic diaphragm muscle became fatigued significantly faster than controls ($P < 0.05$) (Fig. 7A–C), whereas EDL muscle became slightly fatigued, but not significantly faster ($P > 0.05$) (Fig. 7A′–C′). During the early phase of repetitive activation, the forces achieved in transgenic diaphragm muscles declined precipitously and then decreased smoothly and stabilized at 30–45% of the baseline value. The force output of the transgenic diaphragm remained significantly lower than that of the control. Interestingly, the transgenic diaphragm and EDL muscles showed round contractive peaks rather than sharp peaks typical of controls (Fig. 7B,B′,C,C′); the reason for this remains unknown.

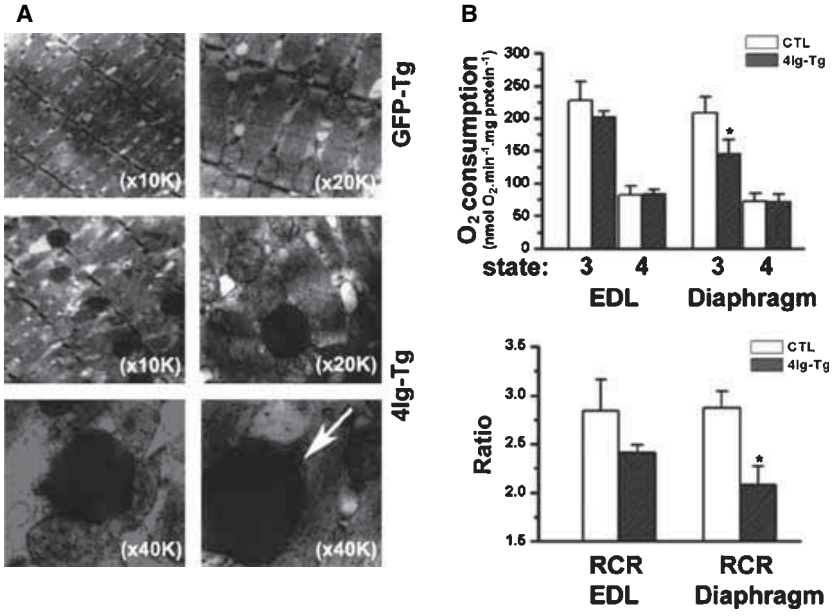

Fig. 5. Localization of 4Ig aggregates in mitochondria and measurements of mitochondrial respiratory activities. (A) Transmission electron microscopy images of 4Ig aggregates in mitochondria of the EDL and diaphragm muscles. The white arrow indicates an incomplete mitochondrial membrane. (B) Upper panel: O_2 consumption measurements during states 3 and 4 with succinate and rotenone substrates. Lower panel: RCR. Open columns: control muscles. Hatched columns: 4Ig-Tg muscles. Values are means ± SE obtained from three mice in each group. *Significant difference from the control group, $P < 0.05$.

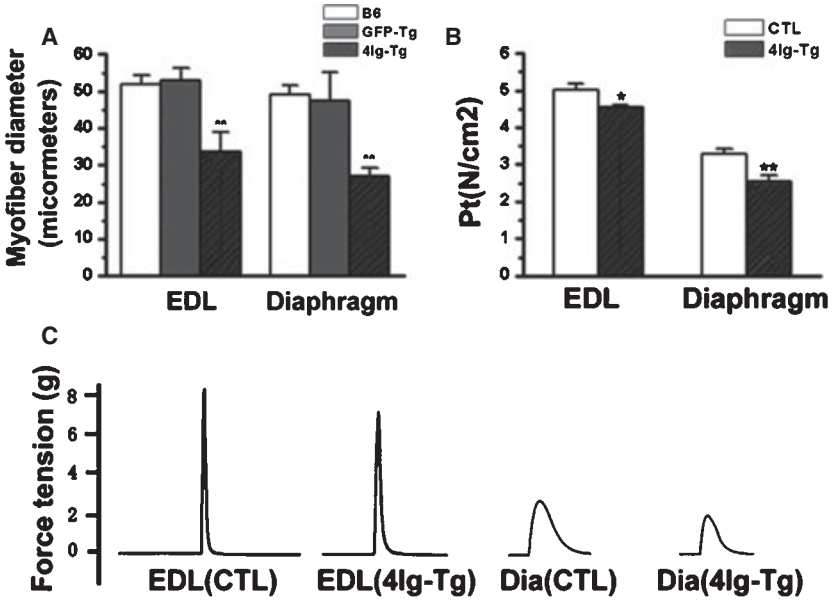

Fig. 6. Force development and structural changes of transgenic muscles. (A) The transgenic muscles were removed from 6-month-old transgenic mice. The thin muscle slides prepared as described in the legend of Fig. 3 were examined under a confocal microscope. The diameters of 200–300 myofibers were measured by LEICA CONFOCAL software, and grouped as either having [57 $BL/_6$ (B6)] and aggregates or not. Diameters of the muscles from 6-month-old GFP transgenic mice were used as controls. (B) The transgenic EDL muscle and diaphragm were removed from 6-month-old transgenic mice. The strength of the contraction forces generated were measured with 10 mA stimuli as described in Experimental procedures. The littermates without 4Ig expression were used as control animals. The data were obtained from three independent experiments. (C) Typical contractions of transgenic muscles.

Discussion

L-MLCK has extra domains in its N-terminal extension, such as 2DFRxxL, tyrosine phosphorylation motif and Ig domains. These domains provide L-MLCK with the structural basis to allow the docking of microfilaments and the regulation of endothelial permeability, and allow the mediation of cytokinesis [10,17,19,20]. To explore potential further functions of L-MLCK, we analyzed its sequences and identified a putative aggregation domain (4Ig) within the N-terminal extension. Its aggregation ability was then verified through both *in vitro* and *in vivo* analysis. The aggregate formed by the 4Ig domain was characterized by: (a) the typical detergent-resistant property of aggregates; (b) a mixture of the 4Ig monomer and cytoskeletal proteins such as actin; and (c) predominant deposition in the mitochondria, where structural impairment resulted. These characteristics are common features of aggregates. In addition, our results ruled

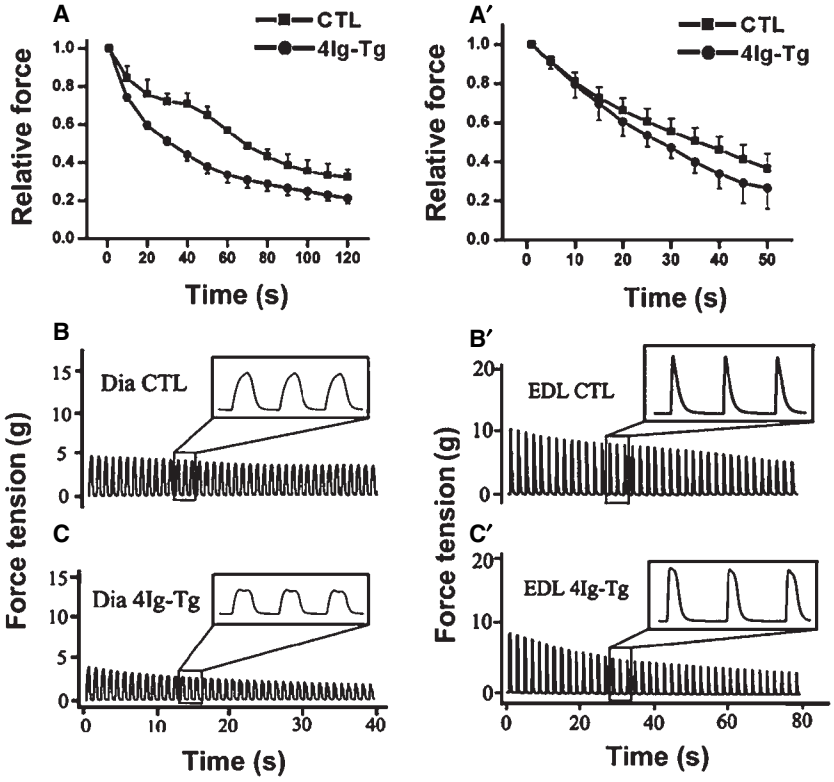

Fig. 7. Fatigue tests for transgenic muscles. (A, A′) (diaphragm and EDL muscle): mean tetanic force (± SEM) during repetitive isometric activation. ■, wild-type; ●, 4Ig-Tg. (B, B′) (diaphragm and EDL muscle) and (C, C′) (diaphragm and EDL muscle) show the contractive curves of control and 4Ig-Tg muscles.

out the possibility that this aggregate was formed only in response to the overexpression of 4Ig proteins. The evidence was as follows. First, 4Ig aggregate formation was independent of expression levels. In line 1 of 4Ig-Tg mice, 4Ig expression in skeletal muscle was much lower than in other lines [such as lines 3, 4 and 6 (Fig. 3)], but clear aggregates could still be detected. Conversely, in lines 2 and 7, 4Ig expression levels were high, and, in the case of skeletal muscle, even higher than that in line 6, yet no aggregate was observed. Second, within the same line, 4Ig expression levels at different periods were comparable but aggregate formation occurred only in older muscles, suggesting that the aggregation was triggered by certain physiological conditions rather than by protein overexpression. Taken together, the above findings indicate that L-MLCK has an aggregation domain within its N-terminal extension.

Investigating how L-MLCK gives rise to aggregate formation is helpful in understanding its potential function. Our results showed that only the 4Ig domain has an aggregation ability, but not intact L-MLCK or other truncated fragments, implying that the aggregation activity is blocked in intact L-MLCK by an unknown mechanism. Release of the 4Ig domain from L-MLCK through proteolytic cleavage may therefore be a necessary step for aggregate formation. In fact, such a mechanism is also adopted in other molecules. For example, amyloid β-protein precursor protein shows its aggregation ability only after cleavage [24,25]. Another important issue is determining what factor triggers aggregate formation. From our data, oxidative stress or reactive oxygen species may be an important factor, as H_2O_2 can induce a high level of 4Ig multimer formation *in vitro*. This speculation is consistent with the fact that 4Ig aggregates localized in the mitochondria, where a burst of oxidative free radicals is produced. Interestingly, HSPs, which possess antiaggregation properties, were found at lower levels both *in vitro* and *in vivo* where 4Ig was expressed. This finding led us to speculate that 4Ig aggregate formation is associated with HSP function. This hypothesis is supported by the observation that extensive aggregate formation occurred in the diaphragms of HSP-deficient bovines [26]. In conclusion, molecular cleavage of L-MLCK, oxidative stress and the reduction in HSP levels may be critical factors for 4Ig aggregate formation. In this work, diaphragm muscle showed more extensive aggregate formation than thigh skeletal muscle. This difference may result from their specific physiological environments, including the level of oxidative stress and contraction activity. For example, the diaphragm may experience long durations of oxidative stress, due to the periodicity of its contractions [27].

Our further study demonstrated that the aggregates formed by 4Ig in skeletal muscle caused a reduction in oxygen consumption, faster fatigue, and evidence of degenerative pathology. These findings imply that L-MLCK may play a role in muscle pathology through aggregate formation. Such a role is consistent with observations that L-MLCK can be both expressed at a high level [28] and cleaved by caspases in response to some pathological signals [29], such as oxidative stress, nuclear factor kappa B [28], tumor necrosis factor-α [29] and apoptotic reagents (our unpublished data). Taking these findings together, we therefore hypothesize that the aggregation-based pathology mediated by L-MLCK may include a cascade of sequential molecular events including pathological stimulation, protein cleavage, a reduction in HSP activity, aggregation in mitochondria, and functional impairment. However, similar to other aggregate-based pathological processes, L-MLCK-mediated aggregation is likely to be a very complicated process that is affected by multiple factors, including protein cleavage, HSP functioning, and protein expression levels. Currently, we do not have a physiologically feasible model with appropriate levels of L-MLCK expression and HSP functioning and a proper triggering mechanism for proteolysis to test the aggregation-based pathological process. The study reported in this article, however, has revealed a novel aggregation domain in L-MLCK, provided a direct link between L-MLCK and aggregation, and suggested a preliminary mechanism for aggregate formation. The physiological or pathological processes mediated by L-MLCK via aggregation will be investigated in our future studies.

The Ig domains comprising the N-terminal extension of L-MLCK belong to the C2-type Ig (Ig-C2) superfamily. The Ig-C2 domains are found extensively in adhesion molecules and in intracellular cytoskeletal proteins, including titin, MyBP-Cm, MyBP-M, MyBP-H, myotilin, and palladin [30–35]. As Ig-C2 domains may serve as molecular spacers and bind to a diversity of ligands, it is believed that they have important physiological and structural significance in cell adhesion and maintenance of the cytoskeleton [36]. These domains are commonly present in multiple copies within a single molecule, and have a typical core-β-sheet structure with high sequence similarity. This structural feature suggests that these Ig domains are at particular risk of forming intractable aggregates [37–39]. Studies on at least two amyloidal diseases involving deposition of Ig domains support the notion that Ig domains are involved in aggregation [40]. Our findings reported in this article provided a direct link between an Ig domain and aggregation. However, Ig-C2 domains do not always cause aggregate formation, even though, as in the case of the 2Ig domain of L-MLCK, they have a typical core-sheet structure buried within their molecule. This feature might be helpful for Ig-containing molecules to display their specific functions while sharing a common structure.

In this work, little transgenic expression of 4Ig was detected in tissues such as the brain and liver. The promoter we used was CMV immediate element 1 (CMVIE). It has been reported that CMVIE activity in transgenic mice varies markedly in different tissues as well as in different lines [41,42]. Thus, the reason for unequal expression of 4Ig in our transgenic lines may be that the CMVIE promoter does not drive 4Ig expression ubiquitously or, operating alone, is not sufficiently efficient. Thus far, we do not know whether 4Ig causes aggregation in other tissues. On the other hand, this tissue-specific expression pattern of 4Ig may help to rule out possible interference from other tissues during phenotypic analysis.

Experimental procedures

Reagents and animals

Restriction enzymes were purchased from Takara Company (Kyoto, Japan), and all antibodies, including secondary antibody and antibody to green fluorescent protein (GFP), were purchased from Santa Cruz Biotechnology (Santa Cruz, CA, USA) or Sigma-Aldrich (St Louis, MO, USA). SPF mice of the C57BL/6, CBA and transgenic lines were maintained at the National Resource Center of Mutated Mice (NRCMM, PR China). The animal protocol was approved by the Institutional Animal Care and Use Committee of the Model Animal Research Center of Nanjing University.

Cell culture and transfection

Murine Colon26 cells (ATCC, Manassas, VA, USA) were maintained in RPMI 1640 (Sigma Chemical Co., St Louis, MO, USA) supplemented with 100 $\mu g \cdot mL^{-1}$ streptomycin, 100 $u \cdot mL^{-1}$ penicillin, 3.7 $mg \cdot mL^{-1}$ sodium bicarbonate and 10% fetal bovine serum (Gibco BRL, Grand Island, NY, USA). Transfections with Lipofectamine 2000 (Invitrogen, Carlsbad, CA, USA) were performed exactly as described in the manufacturer's manual.

Construction of plasmids for L-MLCK variants

The construction of chicken L-MLCK (pEGFP–MLCK210) and of its truncated variants tagged with

EGFP have been described previously [43]. pEGFP251 and pEGFP–4Ig plasmids, which respectively expressed the 2Ig and 4Ig domains driven by the CMV promoter, were derived from pEGFP–MLCK210 as described previously [19]. To prepare the pC3–4Ig construct, the region comprising nucleotides 1279–2466 was amplified by PCR from full-length L-MLCK and subcloned into a pEGFP–C3 vector (Clontech, Palo Alto, CA, USA) via the *Eco*RI/*Bam*HI sites. The primers for the PCR were: P1, 5′-GAA TTC CTC CCC AGT TTG AGA GCC-3′; and P2, 5′-GGA TCC TTA CAG AGA CAC CTG GCA GCT G-3′. The resultant construct was confirmed by sequencing and western blot assay.

Determining the strength of aggregation with western blot

Cells or tissues were lysed in a buffer containing 20 mM Tris/HCl (pH 7.4), 50 mM NaCl, 1% Triton X-100, 1 mM phenylmethylsulfonyl fluoride and 10 $\mu g \cdot mL^{-1}$ aprotinin (Sigma Chemical Co., St Louis, MO, USA) on ice for 30 min. Following this, they were centrifuged at 8064 ***g*** for 10 min, and the pellet (P1) and supernatant (S1) were collected. P1 was further dissolved in lysis buffer containing 2% SDS, and centrifuged for 10 min, and the resultant pellet (P2) and supernatant (S2) were collected. P2 was further dissolved in 70% formic acid. After volatilization, lysis buffer containing 2% SDS was added, the solution was centrifuged for 10 min, and the supernatant (S3) was collected. Supernatants S1, S2 and S3 were used for western blot assay. The proteins were separated using 12% SDS/PAGE gel, and transferred to a polyvinylidene difluoride membrane (MSI, Westboro, MA, USA). The blot was visualized using enhanced chemiluminescence reagents (PerkinElmer Life and Analytical Sciences, Boston, MA, USA).

Production of transgenic mice (Tg-4Ig)

The pC3–4Ig construct was digested with *Apa*LI and *Nae*I, producing a 3.5 kb linearized DNA segment containing a CMV promoter, an EGFP coding region, a 4Ig coding region, and a polyA signal. The DNA (3 $ng \cdot \mu L^{-1}$) was microinjected into the male pronuclei of fertilized eggs from B6CBA females. The injected eggs were then implanted into the oviduct of pseudopregnant foster mothers. The founders were identified by PCR with the following primer pair: P1, 5′-GCCACAAGTTCAGCGTGTCCG-3′; and P2, 5′-GTTGGGGTCTTTGCTCAGGGCG-3′. The founders containing pEGFP–4Ig DNA were used for the further breeding of heterozygous transgenic stable lines by backcrossing with C57BL/6 mice. Transgene integration was confirmed by sequencing, and the expression of the transgene construct in different tissues was determined by western blot assay. In our experiments, eight positive founders and eight stable lines were obtained, of which seven lines expressed 4Ig in the skeletal muscles.

Morphology of the aggregates in muscles

In order to characterize the properties of the aggregation, transmission electron microscopy examinations were performed. Fresh EDL muscles were dissected and fixed with 4% glutaraldehyde (in 0.1 M Milloning's buffer, pH 7.4). The biopsies were then sampled by standard methods for use in electron microscopy (JEOL JEM-1200EX) [44].

Measurement of muscle contraction force

Diaphragm and EDL muscles were prepared for contraction measurement according to the methods of Ingalls *et al.* and Clancy *et al.* [45,46] in order to determine the contractility of aggregate-affected tissues. Briefly, the muscles were mounted on force-displacement transducers (Grass model FT03.C; Grass, Quincy, MA, USA) in a chamber containing Krebs–Ringer buffer (in $mmol \cdot L^{-1}$: NaCl, 137; $NaHCO_3$, 24; KCl, 5; $CaCl_2$, 2; NaH_2PO_4, 1; $MgSO_4$, 0.487; pH 7.4). After 10 min of equilibration at 35–37 °C, the physiological muscle optimal length (L_o) was set with a series of twitch contractions. Muscles were stimulated with two platinum wire electrodes, and the contractive curves were simultaneously recorded with POWERLAB CHART 5.0 software (AD Instruments, Colorado Springs, CO, USA). Stimuli of 10 mA were used to develop an isometric twitch force (P_t). The cross-sectional area (in cm^2) was calculated from the ratio of muscle weight to muscle length at L_o, assuming a muscle density of 1.06 $g \cdot cm^{-3}$. All forces are reported in units of normalized force ($N \cdot cm^{-2}$).

Fatigue test protocol

After measurement of baseline contractile properties, the muscles of 6-month-old mice were stimulated at a frequency giving approximately one-half of the maximal tetanic force. For EDL muscle, 50 tetani (70 Hz, 300 ms duration) were given at intervals of 2 s, giving a duty cycle (tetanic duration divided by tetanic interval) of 0.15 [47]. Fatigue of the diaphragm was determined by using a standard 2 min period of isometric stimulation that employed activation at 40 Hz in bursts of 330 ms duration repeated each second [48].

Measurement of mitochondrial respiratory activity

Isolation of mitochondria from muscles was performed according to a manufacturer's protocol (Beyotime Co., Nantong, China). Mitochondrial respiratory functioning was measured by using a Clark-type oxygen electrode (Hansatech DW 1; King's Lynn, UK). Reactions were

conducted in a 2 mL, closed, thermostatically controlled (25 °C) and magnetically stirred glass chamber containing 0.5 mg of mitochondrial protein in a reaction buffer of 225 mM mannitol, 75 mM sucrose, 10 mM Tris, 10 mM KCl, 10 mM K_2HPO_4, and 0.1 mM EDTA (pH 7.5), in accordance with Tonkonogi's report [49]. After equilibration, mitochondrial respiration was initiated by adding succinate (10 mM) plus rotenone (4 μM). State 3 respiration was determined after adding ADP to a final concentration of 200 μM, and state 4 respiration was measured as the rate of oxygen consumption in the absence of ADP phosphorylation. RCR, the ratio between state 3 and state 4 respiration, was calculated according to Estabrook's method [50]. The value used for oxygen solubility at 25 °C was 253.4 nmol $O_2 \cdot mL^{-1}$.

Data analysis

All results are presented as means ± SEM of *n* observations, unless otherwise noted. Statistical significance was determined at the 95% confidence level using Student's *t*-test for unpaired or paired samples as indicated.

Acknowledgements

We are grateful to Jing Zhang, Pengyu Gu and Jie Bao of MARC core facility for technical assistance with the microinjection. We also thank Professor James Stull of UT Southwestern Medical Center at Dallas for generous help. This work is supported by the National Natural Science Foundation of China (No. 30470852). This work was supported by the MOST of China (Zhu: 2007 CB947100) and 973 program (Gao: 2005CB522501).

References

1 Ikebe M, Hartshorne DJ & Elzinga M (1987) Phosphorylation of the 20,000-dalton light chain of smooth muscle myosin by the calcium-activated, phospholipid-dependent protein kinase. Phosphorylation sites and effects of phosphorylation. *J Biol Chem* **262**, 9569–9573.
2 Kamm KE & Stull JT (1985) Myosin phosphorylation, force, and maximal shortening velocity in neurally stimulated tracheal smooth muscle. *Am J Physiol* **249**, 238–247.
3 Stull JT, Lin PJ, Krueger JK, Trewhella J & Zhi G (1998) Myosin light chain kinase: functional domains and structural motifs. *Acta Physiol Scand* **164**, 471–482.
4 Kamm KE & Stull JT (2000) Dedicated myosin light chain kinases with diverse cellular functions. *J Biol Chem* **276**, 4527–4530.
5 Schoenwaelder SM & Burridge K (1999) Bidirectional signaling between the cytoskeleton and integrins. *Curr Opin Cell Biol* **11**, 274–286.
6 Bresnick AR (1999) Molecular mechanisms of nonmuscle myosin-II regulation. *Curr Opin Cell Biol* **11**, 26–33.
7 Sato M, Tani E, Fujikawa H & Kaibuchi K (2000) Involvement of Rho-kinase-mediated phosphorylation of myosin light chain in enhancement of cerebral vasospasm. *Circ Res* **87**, 195–200.
8 van Nieuw Amerongen GP, Vermeer MA & van Hinsbergh VW (2000) Role of RhoA and Rho kinase in lysophosphatidic acid-induced endothelial barrier dysfunction. *Arterioscle Thromb Vasc Biol* **20**, E127–E133.
9 Jung C, Chylinski TM, Pimenta A, Ortiz D & Shea TB (2004) Neurofilament transport is dependent on actin and myosin. *J Neurosci* **24**, 9486–9496.
10 Clayburgh DR, Rosen S, Witkowski ED, Wang F, Blair S, Dudek S, Garcia JG, Alverdy JC & Turner JR (2004) A differentiation-dependent splice variant of myosin light chain kinase, MLCK1, regulates epithelial tight junction permeability. *J Biol Chem* **279**, 55506–55513.
11 Clayburgh DR, Shen L & Turner JR (2004) A porous defense: the leaky epithelial barrier in intestinal disease. *Lab Invest* **84**, 282–291.
12 Tran QK, Watanabe H, Zhang XX, Takahashi R & Ohno R (1999) Involvement of myosin light-chain kinase in chloride-sensitive Ca2+ influx in porcine aortic endothelial cells. *Cardiovasc Res* **44**, 623–631.
13 Szaszi K, Kurashima K, Kapus A, Paulsen A, Kaibuchi K, Grinstein S & Orlowski J (2000) RhoA and rho kinase regulate the epithelial Na+/H+ exchanger NHE3. Role of myosin light chain phosphorylation. *J Biol Chem* **275**, 28599–28606.
14 Ammit AJ, Armour CL & Black JL (2000) Smooth-muscle myosin light-chain kinase content is increased in human sensitized airways. *Am J Respir Crit Care Med* **161**, 257–263.
15 Aromolaran AS, Albert AP & Large WA (2000) Evidence for myosin light chain kinase mediating noradrenaline-evoked cation current in rabbit portal vein myocytes. *Physiology* **524**, 853–863.
16 Watterson DM, Collinge M, Lukas TJ, Van Eldik LJ, Birukov KG, Stepanova OV & Shirinsky VP (1995) Multiple gene products are produced from a novel protein kinase transcription region. *FEBS Lett* **373**, 217–220.
17 Garcia JG, Lazar V, Gilbert-McClain LI, Gallagher PJ & Verin A (1997) Myosin light chain kinase in endothelium: molecular cloning and regulation. *Am J Respir Cell Mol Biol* **16**, 489–494.
18 Yang CX, Wei DM, Chen C, Yu WP & Zhu MS (2005) 5DFRXXL region of long myosin light chain kinase causes F-actin bundle formation. *Chin Sci Bull* **50**, 2044–2050.
19 Yang CX, Chen HQ, Chen C, Yu WP, Zhang WC, Peng YJ, He WQ, Wei DM, Gao X & Zhu MS (2006) Microfilament-binding properties of N-terminal extension of the isoform of smooth muscle long myosin light chain kinase. *Cell Res* **16**, 367–376.

20 Dulyaninova NG, Patskovsky YV & Bresnick AR (2004) The N-terminus of the long MLCK induces a disruption in normal spindle morphology and metaphase arrest. *J Cell Sci* **117**, 1481–1493.
21 Fernandez-Escamilla AM, Rousseau F, Schymkowitz J & Serrano L (2004) Prediction of sequence-dependent and mutational effects on the aggregation of peptides and proteins. *Nat Biotechnol* **22**, 1302–1306.
22 Zhou W & Freed CR (2004) Tyrosine-to-cysteine modification of human α-synuclein enhances protein aggregation and cellular toxicity. *J Biol Chem* **279**, 10128–10135.
23 Frederikse PH, Garland D, Zigler JS Jr & Piatigorsky J (1996) Oxidative stress increases production of beta-amyloid precursor protein and beta-amyloid (Abeta) in mammalian lenses, and Abeta has toxic effects on lens epithelial cells. *J Biol Chem* **271**, 10169–10174.
24 Ross CA & Poirier MA (2004) Protein aggregation and neurodegenerative disease. *Nat Med* **10**, S10–S17.
25 Milligan CE (2000) Caspase cleavage of APP results in a cytotoxic proteolytic peptide. *Nat Med* **6**, 385–386.
26 Sugimoto M, Furuoka H & Sugimoto Y (2003) Deletion of one of the duplicated HSP70 genes causes hereditary myopathy of diaphragmatic muscles in Holstein–Friesian cattle. *Anim Genet* **34**, 192–197.
27 Clanton TL, Zuo L & Klawitter P (1999) Oxidants and skeletal muscle function: physiological and pathophysiologic implications. *Proc Soc Exp Biol Med* **222**, 253–262.
28 Graham WV, Wang F, Clayburgh DR, Cheng JX, Yoon B, Wang Y, Lin A & Turner JR (2006) Tumor necrosis factor-induced long myosin light chain kinase transcription is regulated by differentiation-dependent signaling events: characterization of the human long myosin light chain kinase promoter. *J Biol Chem* **281**, 26205–26215.
29 Petrache I, Birukov K, Zaiman AL, Crow MT, Deng H, Wadgaonkar R, Romer LH & Garcia JG (2003) Caspase-dependent cleavage of myosin light chain kinase (MLCK) is involved in TNF-alpha-mediated bovine pulmonary endothelial cell apoptosis. *FASEB J* **17**, 407–416.
30 Labeit S, Barlow DP, Gautel M, Gibson T, Holt J, Hsieh CL, Francke U, Leonard K, Wardale J & Whiting AEA (1990) A regular pattern of two types of 100-residue motif in the sequence of titin. *Nature* **345**, 273–276.
31 Einheber S & Fischman DA (1990) Isolation and characterization of a cDNA clone encoding avian skeletal muscle C-protein: an intracellular member of the immunoglobulin superfamily. *Proc Natl Acad Sci USA* **87**, 2157–2161.
32 Noguchi J, Yanagisawa M, Imamura M, Kasuya Y, Sakurai T, Tanaka T & Masaki T (1992) Complete primary structure and tissue expression of chicken pectoralis M-protein. *J Biol Chem* **267**, 20302–20310.
33 Vaughan KT, Weber FE, Einheber S & Fischman DA (1993) Molecular cloning of chicken myosin-binding protein (MyBP) H (86-kDa protein) reveals extensive homology with MyBP-C (C-protein) with conserved immunoglobulin C2 and fibronectin type III motifs. *J Biol Chem* **268**, 3670–3676.
34 Salmikangas P, Mykkanen OM, Gronholm M, Heiska L, Kere J & Carpen O (1999) Myotilin, a novel sarcomeric protein with two Ig-like domains, is encoded by a candidate gene for limb-girdle muscular dystrophy. *Hum Mol Genet* **8**, 1329–1336.
35 Parast MM & Otey CA (2000) Characterization of palladin, a novel protein localized to stress fibers and cell adhesions. *J Cell Biol* **150**, 643–656.
36 Williams AF & Barclay AN (1988) The immunoglobulin superfamily – domains for cell surface recognition. *Annu Rev Immunol* **6**, 381–405.
37 Raffen R, Dieckman LJ, Szpunar M, Wunschl C, Pokkuluri PR, Dave P, Wilkins Stevens P, Cai X, Schiffer M & Stevens FJ (1999) Physicochemical consequences of amino acid variations that contribute to fibril formation by immunoglobulin light chains. *Protein Sci* **8**, 509–517.
38 McParland VJ, Kad NM, Kalverda AP, Brown A, Kirwin-Jones P, Hunter MG, Sunde M & Radford SE (2000) Partially unfolded states of beta(2)-microglobulin and amyloid formation in vitro. *Biochemistry* **39**, 8735–8746.
39 Wright CF, Teichmann SA, Clarke J & Dobson CM (2005) The importance of sequence diversity in the aggregation and evolution of proteins. *Nature* **438**, 878–881.
40 Selkoe DJ (2003) Folding proteins in fatal ways. *Nature* **426**, 900–904.
41 Furth PA, Hennighausen L, Baker C, Beatty B & Woychick R (1991) The variability in activity of the universally expressed human cytomegalovirus immediate early gene 1 enhancer/promoter in transgenic mice. *Nucleic Acids Res* **19**, 6205–6208.
42 Baskar JF, Smith PP, Nilaver G, Jupp RA, Hoffman S, Peffer NJ, Tenney DJ, Colberg-Poley AM, Ghazal P & Nelson JA (1996) The enhancer domain of the human cytomegalovirus major immediate-early promoter determines cell type-specific expression in transgenic mice. *J Virol* **70**, 3207–3214.
43 Poperechnaya A, Varlamova O, Lin PJ, Stull JT & Bresnick AR (2000) Localization and activity of myosin light chain kinase isoforms during the cell cycle. *J Cell Biol* **151**, 697–708.
44 Engel AG (1994) The muscle biopsy. In *Myology* (Engel AG & Franzini-Amstrong B, eds), pp. 822–831. McGraw-Hill, New York, NY.
45 Clancy JS, Takeshima H, Hamilton SL & Reid MB (1999) Contractile function is unaltered in diaphragm from mice lacking calcium release channel isoform 3. *Am J Physiol* **277**, R1205–R1209.

46 Ingalls CP, Warren GL, Williams JH, Ward CW & Armstrong RB (1998) EC coupling failure in mouse EDL muscle after in vivo eccentric contractions. *J Appl Physiol* **85**, 58–67.
47 Dahlstedt AJ, Katz A, Wieringa B & Westerblad H (2000) Is creatine kinase responsible for fatigue? Studies of skeletal muscle deficient of creatine kinase. *FASEB J* **14**, 982–990.
48 Watchko JF & Sieck GC (1993) Respiratory muscle fatigue resistance relates to myosin phenotype and SDH activity during development. *J Appl Physiol* **75**, 1341–1347.
49 Tonkonogi M, Walsh B, Svensson M & Sahlin K (2000) Mitochondrial function and antioxidative defence in human muscle: effects of endurance training and oxidative stress. *J Physiol* **528**, 379–388.
50 Estabrook R (1967) Mitochondrial respiratory control and the polarographic measurement of ADP/O ratios. *Methods Enzymol* **10**, 41–47.